ACS APPLIED MATERIALS & INTERFACES

Research Article

www.acsami.org

Superior Performance of Copper Based MOF and Aminated Graphite Oxide Composites as CO_2 Adsorbents at Room Temperature

Yunxia Zhao,[†,‡] Mykola Seredych,[†] Qin Zhong,[‡] and Teresa J. Bandosz*[,†]

[†]The City College of New York, 160 Convent Avenue, New York, New York 10031, United States

[‡]School of Chemical Engineering, Nanjing University of Science and Technology, Nanjing, 210094 PR China

Supporting Information

ABSTRACT: New composites Cu-BTC MOF and graphite oxide modified with urea (GO-U) are developed and tested as CO_2 adsorbents at room temperature. The composite containing GO-U with the highest nitrogen content exhibits an excellent CO_2 uptake (4.23 mmol/g) at dynamic conditions. The incorporation of GO-U into MOF changes the chemistry and microstructure of the parent MOF and results in synergistic features beneficial for CO_2 retention on the surface. To identify these features the initial and exhausted materials were extensively characterized from the points of view of their porosity and chemistry. Although the adsorption forces are relatively strong, the results indicate that CO_2 is mainly physisorbed on the composites at dry dynamic conditions at ambient temperature and pressure. The primary adsorption sites include small micropores specific for the composites, open Cu sites, and cage window sites.

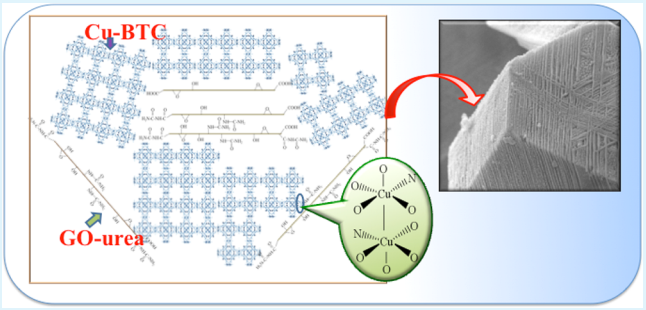

KEYWORDS: *graphite oxide, urea, metal organic framework, composites, CO_2 adsorption*

INTRODUCTION

Carbon dioxide has been recognized as a leading cause of global warming.[1,2] Fossil-fuel-burning power plants are one of the major anthropogenic emission sources.[3] The control of CO_2 emissions is an important challenge facing contemporary society, and thus CO_2 sequestration became a strategic topic related to energy production and consumption.[4−7]

Adsorption is one of the effective postcombustion methods of CO_2 sequestration owing to its low energy requirements and a relatively simple technology.[8] It is well-known that the adsorption process can follow either purely physical or chemical paths. The former employs van der Waals forces between an adsorbent and an adsorbate molecule,[4] while the latter is based on the reaction of an adsorbent with an adsorbate.[9] Recently reactive adsorption has been defined as the physical adsorption process followed by the reactions of an adsorbed species either with an adsorbent surface or between molecules in an adsorbed phase.[10] When separation takes place from ambient air it is quite often that other coadsorbed species such as water or oxygen actively contribute to the reactions occurring in the pore system.[11−13] As for any adsorptive separation process, choosing an efficient CO_2 adsorbent is of paramount importance.[3]

Metal organic frameworks (MOFs) are microporous crystalline solids with well-defined structure.[14,15] Owing to their porosity, they have been widely used for gas adsorption and separation.[16−18] MOFs generally consist of three-dimensional organic−inorganic hybrid networks formed by multiple metal−ligand bonds.[19] Cu-BTC also referred to as HKUST-1[20] is one of the typical MOF materials. It is formed by coordination between metal centers (Cu^{2+}) and organic ligands ($C_6H_3(CO_2)_3$).[20] Extensive studies have been carried out on its gas storage and separation performance.[21−23] Chaffee and co-workers evaluated the CO_2 capacity and CO_2/N_2 selectivity in a PSA system.[24] Their Cu-BTC samples adsorbed up to 12.7 mol/kg CO_2 at 25 °C and 15 bar. The CO_2/N_2 selectivity of Cu-BTC at 25 °C was reported to be about 20, and it decreased slowly with an increase in the pressure. Yang and co-workers reported the adsorption capacity of Cu-BTC for CO_2 as 69 mL/g (3.08 mmol/g) at 22 °C and 0.98 p/p_0.[25] They indicated that the CO_2 adsorption capacity does not significantly decrease in the presence of common flue gas components such as SO_2 and NO. Taking into account the reported high thermal and structural stability of Cu-BTC and its excellent performance as the CO_2 adsorbent, this MOF is considered as one of the promising separation media for CO_2 capture from flue gas.[23−26]

To further enhance CO_2 adsorption, various modifications have been applied to MOFs. They include ion doping,[27,28] formation of MOF-inorganic species (such as carbon nanotube, graphite oxide, and silica) composites[29,30] and functionalization of the ligands.[18,31] Snurr and co-workers reported that CO_2 uptake and its selectivity over N_2 and CH_4 in Cu-BTC significantly increased in the presence of water molecules coordinated to open-metal sites in the framework.[26] Yang and

Received: February 24, 2013
Accepted: May 16, 2013
Published: May 16, 2013

   dx.doi.org/10.1021/am4006989 | ACS Appl. Mater. Interfaces 2013, 5, 4951−4959

co-workers prepared the hybrid Li@CNT@[$Cu_3(btc)_2$], which was formed by the combination of Li doping and carbon nanotube incorporation. On this material CO_2 and CH_4 uptakes 0.77 mg/m^2 and 0.15 mg/m^2 per an effective specific surface area at 298 K and at 18 bar increased about 305% and 200%, respectively, compared to the unmodified MOF.[32]

Recently, our group has investigated MOF and graphite oxide (GO) composites as adsorbents of NH_3,[33] H_2S,[34] and NO_2.[13] The synergistic effects related to the chemistry of these composites formation provide active sites for reactive adsorption.[12,35] These sites were formed at the interface between the GO layers and MOF components. This kind of materials has been investigated as a CO_2 adsorbent by Liu and co-workers.[36] They found that the formation of the composite enhanced the amount of carbon dioxide adsorbed of about 30% (8.26 mmol/g as adsorbed at equilibrium at 1 atm and 0 °C) in comparison with MOF alone. To further extend the scope of the synergistic composite features, we synthesized the composites of Cu-BTC with aminated graphite oxide.[37] This specific chemistry of the GO component was chosen since the target adsorbate this time is CO_2 and its interactions with amine groups incorporated to various materials have been broadly investigated.[38−40] Therefore the objective of this paper is the detailed evaluation of these new materials as CO_2 adsorbents at room temperature taking into account the synergistic surface features specific only for these composites.[37] The adsorption mechanism is explored based on the extensive characterization of the adsorbents before and after CO_2 exposure.

EXPERIMENTAL SECTION

Materials. The detailed synthesis procedure of graphite oxide (GO) and Cu-BTC was described elsewhere.[11,20,35,41] Briefly, the aminated graphite oxide was prepared by mixing 1 g GO and different amount of urea in 100 mL H_2O and stirring for 24 h. The products were washed with water to remove excess of unreacted urea, air-dried after filtering, and referred to as GO-U1, GO-U2, and GO-U3. The urea concentrations used for GO modifications were 0.030, 0.150, and 0.300 mol/L, respectively.

The preparation of Cu-BTC[20] and GO-U composites was done as described in detail in ref 37. GO-U and the MOF components were simultaneously dispersed/dissolved in the solvent by sonication thus the MOF units were allow to grow in the presence of GO-U in the reaction vessel. The content of GO-U was 10 wt % of the parent Cu-BTC weight. The composites are referred to as MOF/GO-U1, MOF/GO-U2, and MOF/GO-U3 for the different GO-U samples. For comparison, the MOF/GO composite was also synthesized[42] and used as CO_2 adsorbent.

Methods. *CO_2 Dynamic Adsorption.* Assessment of the CO_2 adsorption capacity on the samples at atmospheric pressure was carried out using a TA Instruments. About 20 mg of the adsorbent MOF/GO-U was placed in a small pan, heated up to 110 °C at a heating rate of 10 °C/min under pure N_2 flow (100 mL/min), and held isothermally for 2 h. The temperature was then decreased to 30 °C. At this stage, the sample was saturated by N_2. Then the gas was switched to pure CO_2 50 mL/min and the sample was held isothermally at 30 °C for 2 h. The weight increase (with high accuracy to three decimal places) during this stage was considered as the amount of CO_2 adsorbed.

Heats of CO_2 Adsorption. Heats of CO_2 adsorption were measured using the Calvet type DSC (calorimetric detector-3D sensor) (Setaram Instrumentation, Caluire, France). First, the sample was heated up to 110 °C at a heating rate of 2 °C/min under pure N_2 flow (100 mL/min) and held isothermally for 2 h. The temperature was then decreased to 30 °C at a rate of 2 °C/min. Then pure CO_2 (50 mL/min) was passing through the sample isothermally with a continuous flow of N_2. The heat flow over time curve was recorded. The heat of CO_2 adsorption in joules per gram was calculated by integration of the peaks in the curve.

FTIR. FTIR spectroscopy was carried out using a Nicolet Magna-IR830 spectrometer according to the attenuated total reflectance method (ATR). The experiments were done on the powdered samples, without KBr addition. The composite samples were dried at 120 °C for 12 h before the experiments.

Nitrogen Adsorption. Nitrogen adsorption isotherms were measured using an ASAP 2020 analyzer (Micromeritics, Norcross, GA, USA) at −196 °C. Prior to the experiment, the samples were degassed at 120 °C overnight. The surface area S_{BET}, the total pore volume V_t, the micropore volume V_{mic} (Dubinin−Radushkevich method), and the mesopore volume V_{mes} were obtained from the isotherms. The pore size distributions were calculated using the density functional theory (DFT) method.[43] Even though the exact surface model for our composite are not developed, using the existing model for the series of samples can bring some valuable information and the trend of the changes in the samples' porosity.

Thermal Analysis. Differential thermogravimetric (DTG) curves were obtained using a TA Instruments thermal analyzer (New Castle, DE, USA). The samples were tested from 30 to 1000 °C, with a heating rate of 10 °C/min under a nitrogen flow held at 100 mL/min.

EDX. Electron-dispersive X-ray spectroscopy (EDX) analysis was done at magnification 10 KX with an accelerating voltage of 15.00 kV. A Cu atomic concentration is the average data calculated from four different spots of adsorbent surface analyzed by EDX.

RESULTS AND DISCUSSION

The isothermal (30 °C) CO_2 adsorption profiles of the GO-U, MOF, MOF/GO, and MOF/GO-U composites are presented in Figure 1. The majority of the adsorbents start to saturate

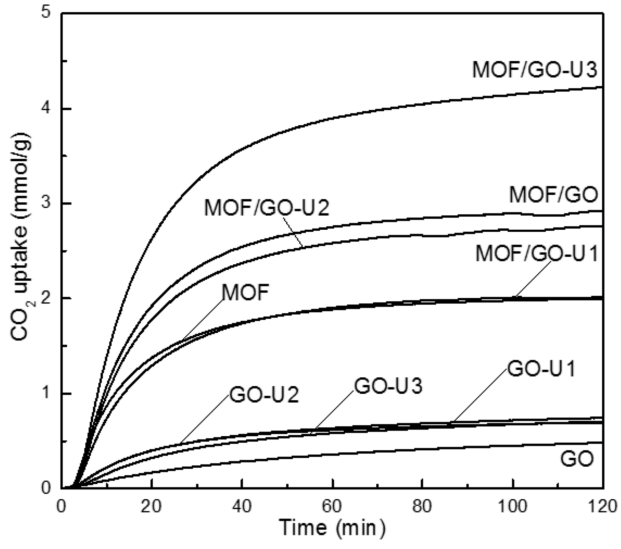

Figure 1. Isothermal (30 °C) CO_2 adsorption profiles of GO-U and MOF/GO-U series.

after 40 min and then the adsorption rates slow. The CO_2 uptakes on all samples after the 2 h testing process are compared in Figure 2. Even though the amounts adsorbed cannot be considered as measured at equilibrium, the shape of the adsorption profiles for all samples indicate that some level of quasi-saturation was reached. After modification with urea, the capacity of GO for CO_2 adsorption increased, which is linked to the introduction of reactive adsorption sites on the amino groups. The content of nitrogen in GO-U1, GO-U2, and GO-U3 is 0.21, 0.41, and 0.59%, respectively.[37] The amount of

dx.doi.org/10.1021/am4006989 | ACS Appl. Mater. Interfaces 2013, 5, 4951−4959

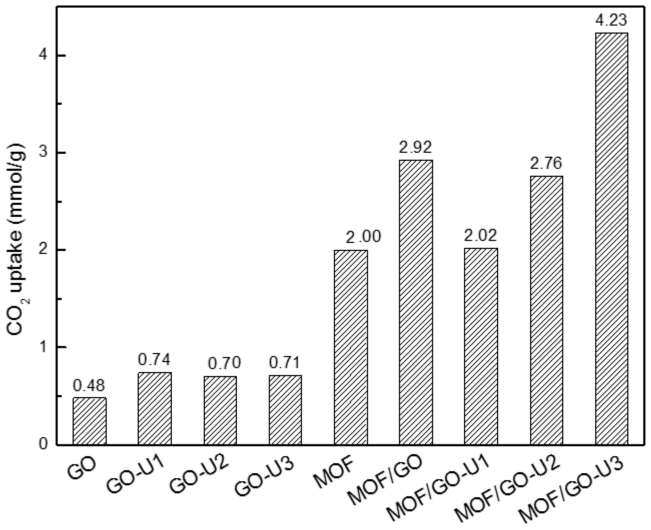

Figure 2. Comparison of the CO_2 uptake on the samples studied after the 2 h testing process.

nitrogen in the composites was not analyzed taking into account that only fraction of nitrogen from GO-U can exist there (10% of the fraction of percent) and traces of nitrogen containing solvent can affect the apparent measurement results. The detailed mechanism of the composite formation and their surface properties are addressed in ref 37. Here, for the sake of discussion, we only briefly reintroduce the important surface features (see the Supporting Information). It is plausible to assume that chemisorption of CO_2 on the amino sites of modified GO follows reactions 1 and 2.[44] Since the molar amounts of those urea-originated sites are certainly much less than the amount of CO_2 adsorbed, reaction 1 is likely to predominate on these sites. Interestingly, all three GO-U samples have the similar CO_2 uptake. This, along with the small amount of nitrogen, suggests that the main contribution of adsorption is from the physical adsorption. It consists of interactions between the delocalized π aromatic system of GO and the molecular quadrupole of CO_2[45] and polar interactions of CO_2 with the oxygen groups on the basal planes. The latter process results in the intercalation of CO_2 between the modified GO layers.[46,47] That process can be more pronounced when more oxygen is present in the interlayer space.

$$—NH_2 + CO_2 \leftrightarrow —NH_2{}^+COO^- \quad (1)$$

$$—NH_2 + —NH_2{}^+COO^- \leftrightarrow —NHCOO^- + —NH_3{}^+ \quad (2)$$

All composites are better CO_2 adsorbents than is the parent MOF. Moreover, the performance improves with an increase in the extent of urea modification. MOF/GO-U3 has the highest CO_2 uptake, 4.23 mmol/g, which is higher than the amounts reported in the literatures and measured at similar conditions on Cu-BTC,[25] on porous carbon monoliths with incorporated Cu-BTC,[48] and on acidic derivative of zeolite SSZ-13.[49] On those materials 3.08, 2.75, and 3.98 mmol/g were reported, respectively. Moreover, on zeolite-templated N-doped microporous carbon 4.4 mmol CO_2/g were adsorbed at thermodynamic equilibrium at ambient temperatures.[50] CAU-1 MOF modified with amines was reported to adsorb CO_2 7.2 mmol/g at 0 °C and 1 atm, 4 mmol/g at 25 °C.[51] On mixed matrix membranes with incorporated size-reduced Cu-BTC, 6.5 mmol/g of CO_2 was adsorbed at equilibrium at 30 °C and 1 bar.[52] In our work, the samples were heated at 110 °C for 2 h and cooled down to 30 °C for about 2 h under N_2 before CO_2 adsorption, so the samples used for CO_2 adsorption were presaturated with nitrogen. Since the selectivity for CO_2 adsorption is reported to be higher than that for N_2 on MOFs,[25] the actual amounts of CO_2 adsorbed in the absence of nitrogen are expected to be higher than those presented in Figure 2. This is owing to the larger quadrupole moment of CO_2 than that of N_2.[53] Even though at our experimental conditions CO_2 is expected to replace nitrogen, the mass of adsorbent taken for calculation includes preadsorbed nitrogen.

The amounts of CO_2 adsorbed on the composites are up to 100% higher than that on the parent MOF. To understand the factors governing the superior performance of these new materials a detailed surface characterization of the initial and exhausted samples was carried out. The comparison of the surface areas and pore volumes is presented in Table 1. The values of the parameters of porous structure increase with an increase in the extent of urea modification of GO. The surface area of MOF/GO-U3 is much higher than that of MOF/GO, which emphasizes the beneficial effect of the GO treatment applied. This new porosity is created at the interface between the graphene layers and the MOF "blocks", and it is the result of the interactions between the oxygen groups and amino groups of GO or GO-U with the unsaturated metal sites of Cu-BTC.[42,54] Formation of composites and the existence of the GO-U scaffolds in the bulk structure of materials also results in an increase in the volume of mesopores, which are important for the transport of CO_2 to its high-energy adsorption sites. The pore size distributions (Figure S1 of the Supporting Information) show the development of pores with sizes of about 5−7 Å in the composites of GO-U with MOF, especially for MOF/GO-U3. Pores of these sizes should be important for the enhanced physical adsorption of CO_2.

Table 1. Parameters of Porous Structure for the MOF, MOF/GO, and MOF/GO-U

sample	S_{BET} (m^2/g)	V_t (cm^3/g)	V_{mic} (cm^3/g)	V_{mic}/V_t (%)
MOF	892	0.428	0.379	89
MOF/GO	1010	0.491	0.436	89
MOF/GO-U1	864	0.421	0.368	87
MOF/GO-U2	936	0.466	0.406	87
MOF/GO-U3	1367	0.663	0.572	86

To visualize the importance of porosity on the CO_2 adsorptive performance, the dependence of the amount adsorbed on the surface area and volume of micropores (assuming that they are one of the highest energy adsorption centers) was analyzed. As seen in Figure 3, well-marked linear trends support the hypotheses on the physical adsorption as the main mechanism of CO_2 retention on our materials. Support for this is the fact that the capacity measured on MOF/GO without any amination also follows this trend. Nevertheless the extent of the increase in porosity of the composites rather cannot account for the 100% increase in CO_2 adsorption capacity on MOF/GO-U3.

Figure 4 presents the hypothesized structure of the MOF/GO-U composites. The X-ray diffraction patterns (Figure S2 of the Supporting Information) show only very slight disturbance in the crystallinity level of MOF units.[37] The copper sites of Cu-BTC and the functional groups of GO and GO-U, like the epoxy, hydroxyl, carboxyl, and amino functionalities are

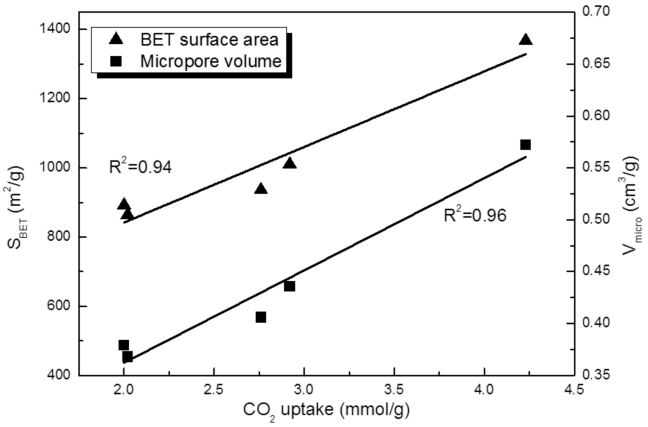

Figure 3. Dependence of the amount adsorbed on the surface area and volume of micropores.

involved in chemical reactions. The oxygen coordination sites available in Cu^{2+} dimers can be replaced by oxygen atoms from GO surface or nitrogen atoms from aminated GO surface.[37] These reactions lead to the formation of additional pores in the parent MOF materials. The surface topography image of MOF/GO-U3 (Figure 4) shows "lacelike" structures in the vicinity of graphene layers embedded within MOF crystals.[37] The kinetic diameter of CO_2 is 3.3 Å, and new pores formed in MOF/GO-U3 material have diameter of about 6 Å (Figure S1 of the Supporting Information).[37] These pores should be the high energy adsorption centers for CO_2. The involvement of amino groups and the different bond length of Cu−O and Cu−N should not only affect the MOF structure but should also generate more unsaturated metal ions since they might be sterically hindered by the presence of GO units from the involvement in coordination chemistry.

Even though the porosity seems to be the main factor governing the CO_2 retention on our composites, the huge increase in the amount of CO_2 adsorbed on the composites in comparison with that on MOF suggests that some specific interactions imposed by surface chemistry of MOF and specific physical and chemical properties of the CO_2 molecule can also play a role in the adsorption process. This chemistry might be related either to the presence of amino groups or to the unsaturated copper sites. As mentioned above, the intended content of GO-U in the composites is only 10 wt % and taking into account the small content of nitrogen in the urea modified GOs, the amount of amines in the total composition of the new materials is rather limited. Therefore changes in the surface acid−base properties, demonstrated as a decrease in pH from 4.46 for MOF to 4.19 for MOF/GO-U1, 4.31 for MOF/GO-U2, and 4.34 for MOF/GO-U3, could be either the result of the synergistic effects of the reactions of these amine groups with BTC and copper centers or of the increase in the presence of the open uncoordinated copper centers. As proposed by Zhou and co-workers[55] and Wu and co-workers,[56] CO_2 primary adsorption sites include the open Cu site and the cage window site. In the latter framework−CO_2 interactions are governed by van der Waals (vdW) forces. The electrostatic interaction between the open metal ion and the CO_2 quadrupole is considered as stronger than a typical vdW interaction.[56] Thus it is proposed that CO_2 is preferentially adsorbed as a O═C═O···Cu configuration, and other sites are populated after the Cu sites are nearly fully occupied.[55] The results obtained by Wu and co-workers also suggest that CO_2 is physically adsorbed on copper sites since the small degree of O−C−O bond bending was found.[56] Since the atomic percent of copper on the surface of our composites (8.3% for MOF, 11.6% for MOF/GO, 12.0% for MOF/GO-U1, 13.4% for MOF/GO-U2, and 13.7% for MOF/GO-U3, respectively)[37] increased with an increase in the extent of GO-urea modification used as the composite component, the plausible explanation of the adsorption mechanism is the combined effect of the open copper sites and the new porosity formed in the composites.

Analyzing the surface chemistry and structure of the materials after CO_2 adsorption should provide more evidence to support the hypothesized above adsorption mechanism. The FTIR spectra are collected in Figure 5. Some changes in the samples' chemistry after CO_2 adsorption are visible. For the GO and GO-U series, a decrease in the intensity of all bands is noticed. Because water from the initial GO or GO-U samples was removed from the surface before the CO_2 adsorption test, wide bands at 3000−3650 cm^{-1} attributed to the hydroxyl stretching vibration of water[57] and the bands present at 1630 cm^{-1} representing deformations of the O−H bond in water[58] decrease distinctly in their intensity after the CO_2 adsorption test. Another obvious change after CO_2 adsorption is the right shift of the band at about 1630 cm^{-1} linked to deformations of the O−H bond, which indicates the reaction of H_2O and CO_2 or strong hydrogen bonds interactions of hydroxyl with CO_2. In addition, the bending vibration of N−H at 1683 cm^{-1} is also in this range. The reaction between amino groups and CO_2 is also

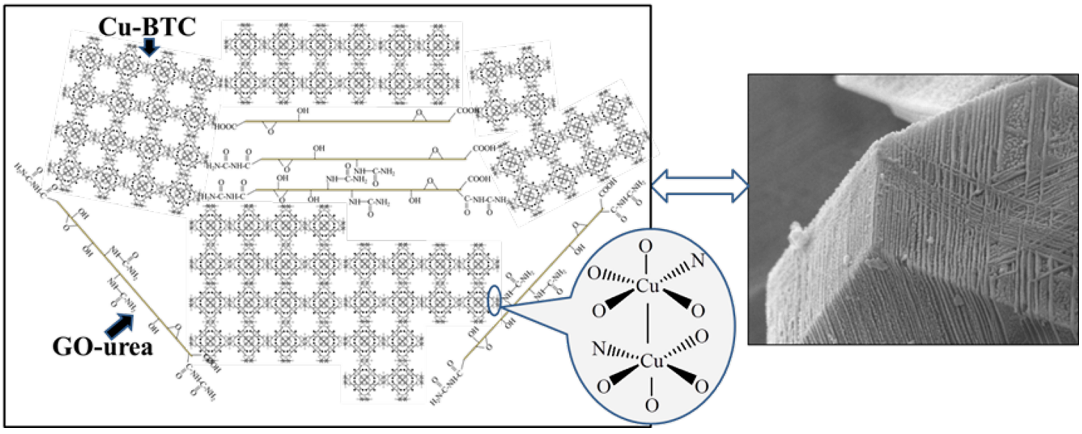

Figure 4. Schematic view of the MOF/GO-U composite structure and the SEM surface topography image of MOF/GO-U3.

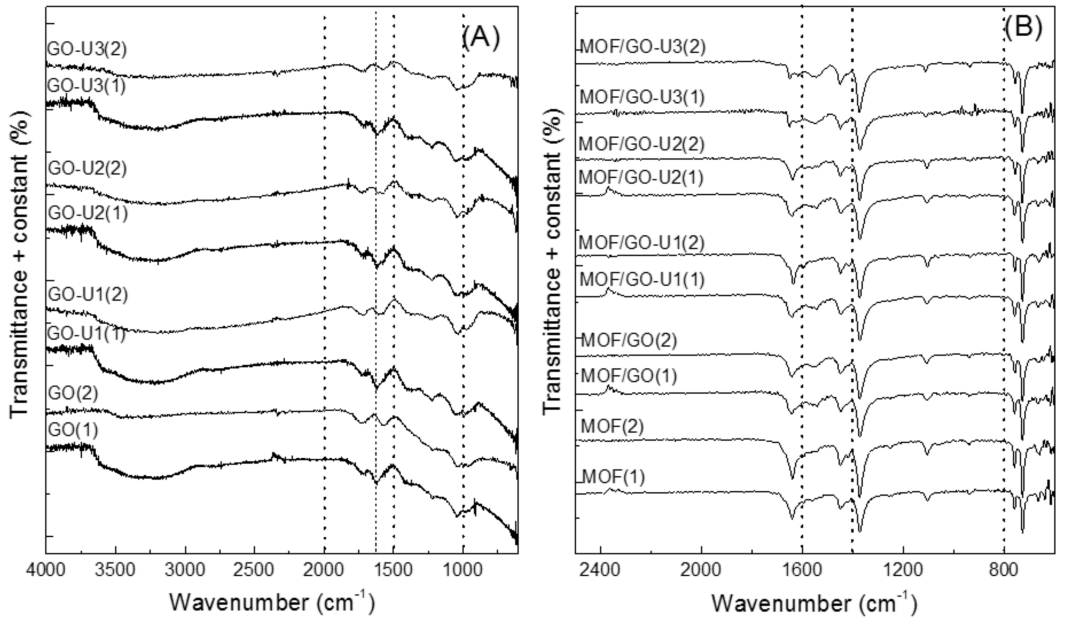

Figure 5. FTIR spectra for the GO-U (A) and MOF/GO-U series (B) of samples: (1) before adsorption, (2) after adsorption.

likely to cause the shift of this band. Some CO_2 on the surface is seen at about 2300 cm^{-1} as a typical band representing asymmetric stretching vibration of CO_2.[59]

For the MOF/GO-U series of samples, the wavenumber is limited to 2500 cm^{-1} because spectra are featureless at 2500−4000 cm^{-1} (Figure 5B). For the initial samples, the artificial increase in the intensity of the band at 2350 cm^{-1} is observed as a result of the applied baseline correction for the presence of atmospheric CO_2. Interestingly, after exposure to CO_2 this feature disappears, which might suggest the presence of carbon dioxide on the surface. Another small change is visible on the spectra between 700 and 600 cm^{-1}. In this range, some peaks disappear or shift slightly after the exposure to CO_2. The bands below 1300 cm^{-1} represent vibrations of the BTC ligand.[42,57] The coordination of CO_2 to the open Cu sites brings a minimal impact on the environment of these BTC ligands. Since carbonates exhibit vibrations at the same range as carboxyl groups,[60,61] their presence cannot be unambiguously confirmed.

To further investigate whether or not CO_2 adsorption imposed any changes in surface chemistry thermal analyses were carried out on the initial and exhausted samples. The DTG curves are shown in Figure 6. Even though the experiments were run up to 1000 °C, the data over 600 °C is not included owing to the featureless DTG curves at higher temperatures. The first peak at about 100 °C is related to the removal of physically adsorbed water.[62] For GO and GO-U after CO_2 adsorption, the intensity of this peak decreases greatly, because water is removed by N_2 purging. The second peak is linked to the decomposition of epoxy groups[63] and $-NH_2$ moiety.[64] It slightly increases in intensity after CO_2 exposure suggesting its reactive adsorption on GO-U3.

On the DTG curves for the MOF, MOF/GO, and MOF/GO-U samples, no marked changes in the weight loss patterns after CO_2 adsorption are visible. This indicates a weak retention of CO_2. As reported in the literature,[55,56] CO_2 is mainly physisorbed on the cage window site and the open Cu site, and its release from these sites should be relatively easy. Interestingly, for MOF/GO-U2 and MOF/GO-U3, the peak before 100 °C becomes more intense after CO_2 adsorption. Those two samples have the largest amounts of unsaturated copper sites and the highest porosity, and they are the best CO_2 adsorbents. We link this increase in weight loss to the CO_2 adsorption on the unsaturated copper sites, which is expected to be stronger than that in the small pores system. For these samples, the peaks on DTG curves near 200 °C decrease in their intensity after CO_2 adsorption. This might be the result of the involvement of water in carbonate formation. The thermal stability of copper carbonates is low.[65,66] For MOF/GO-U2 after CO_2 loading, the sharp peak representing decomposition of carboxylic groups at about 300 °C[35,67] shifts to lower temperature, which shows the mentioned above (Figure 5B) impact of the coordination of CO_2 to the open Cu sites on the environment of the BTC ligands.

The evaluation of adsorption heats is an important tool to understand the mechanism of a gas retention process. The heat flow curves for all samples are present in Figure 7. The adsorption process was exothermic. For simplification of our analyses, two main adsorption sites are distinguished. One group of sites is represented by a sharp narrow peak at the beginning of the adsorption process. Even though the amount adsorbed on these sites is relatively small, the energetic effect is high. We link these sites either to the presence of polar group in the modified GO or to the presence of unsaturated copper sites. On both types of centers CO_2 is expected to adsorb via specific forces. An initial sharp spike in the energetic effect of adsorption is followed by a less intense effect, which is seen on the heat flow curves as a second broad peak. The fact that almost linear decrease in the heat is found in the case of GO suggests the gradual occupation of adsorption sites via their direct interactions with CO_2. The interaction scenario seems to be very specific for MOF/GO-U3 where the maximum on the heat release curves for the secondary adsorption centers is clearly noticed. These centers are in fact the predominant CO_2 adsorption centers. We link this behavior to the kinetic limitations in the accessibility of the very small pores (likely those with sizes 5−7 Å) on the interface between two components of the composite. The maximum in the heat is noticed when the CO_2 is able to access these centers. The

dx.doi.org/10.1021/am4006989 | ACS Appl. Mater. Interfaces 2013, 5, 4951−4959

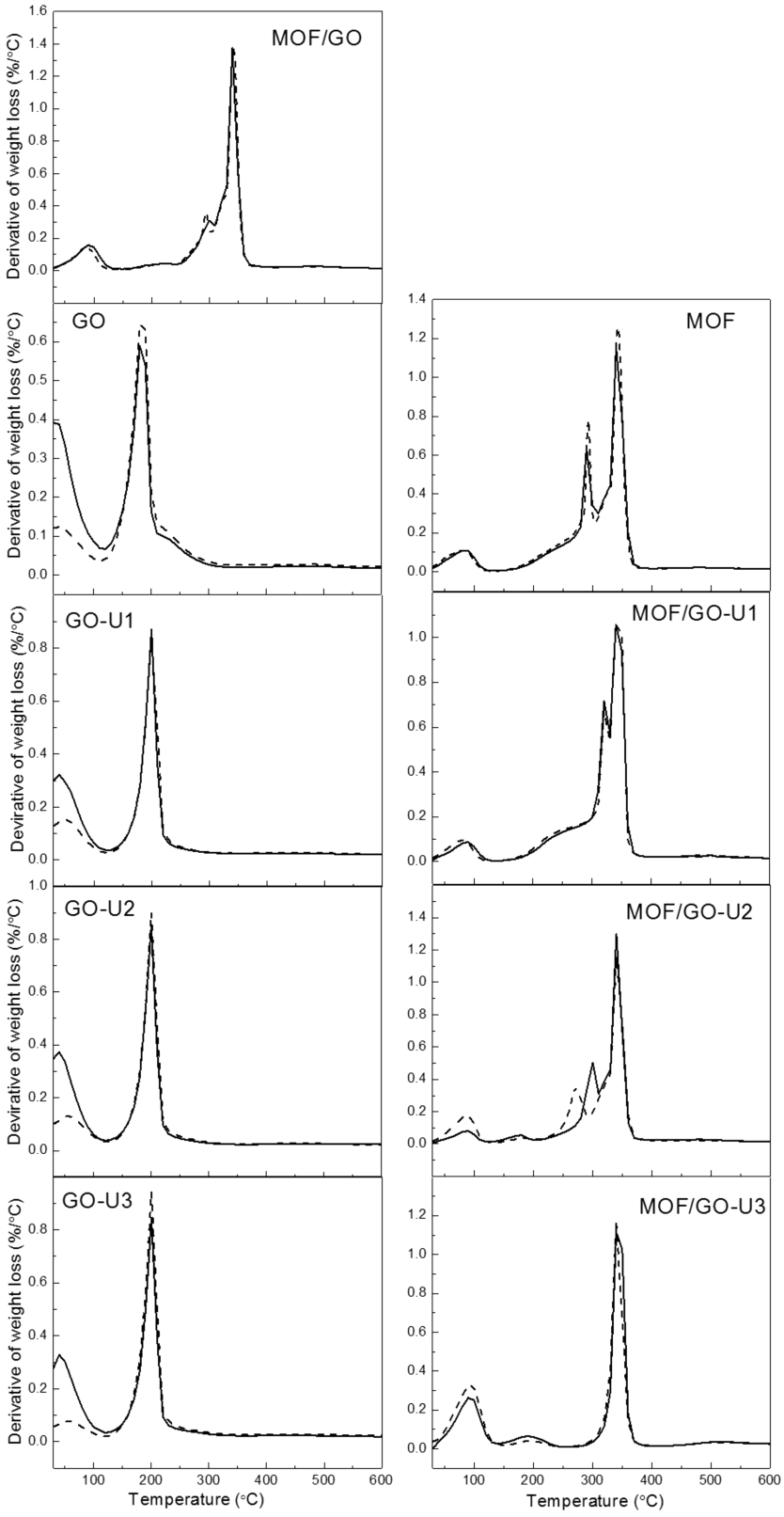

Figure 6. DTG curves of GO-U and MOF/GO-U series of samples before (solid lines) and after (dashed lines) CO_2 adsorption.

extent of these limitations decreases with a decrease in the volume of very small pores.[37] The almost linear gradual decrease in the heat effect is noticed for other two composites as a result of the progress in a not-restricted adsorption on the sites of the same/similar energy.

Figure 8 represents the comparison of the heats released, assuming the presence of two adsorption sites in all materials. This approach can give us the rough estimation of the extent of intensive and extensive factors of the adsorption process. Taking into account that the values reported in Figure 8

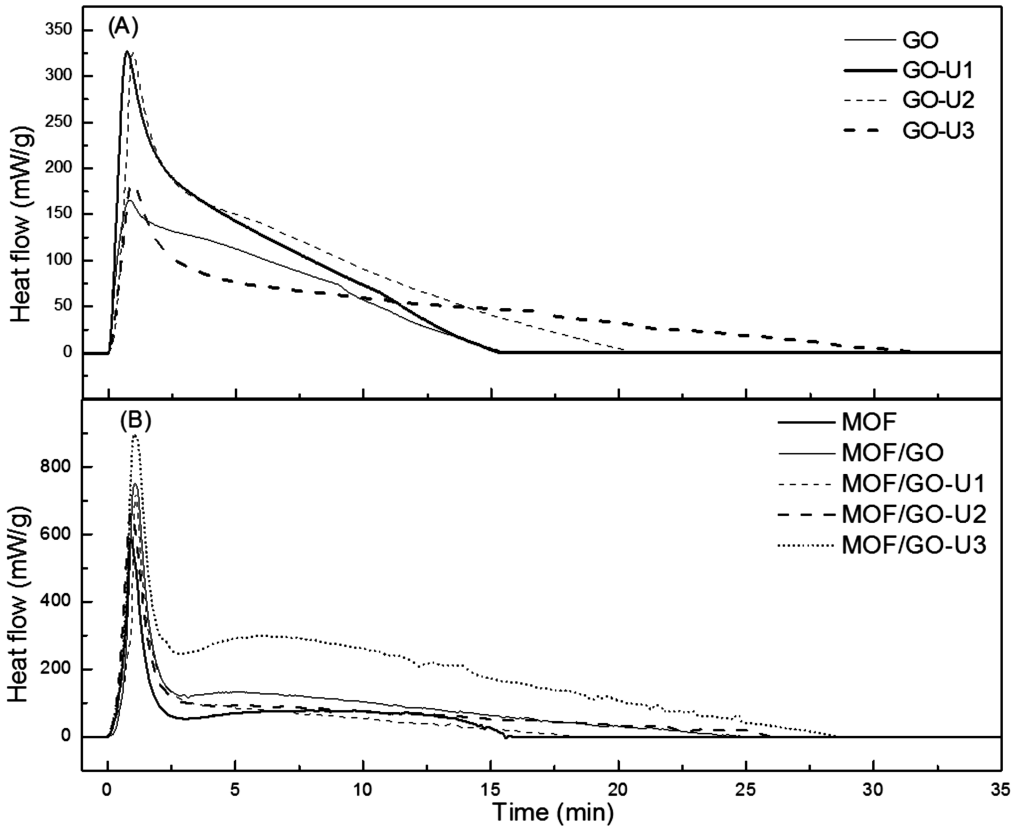

Figure 7. Heat flow versus time curves for CO_2 adsorption on the GO samples (A) and the MOF/GO-U samples (B).

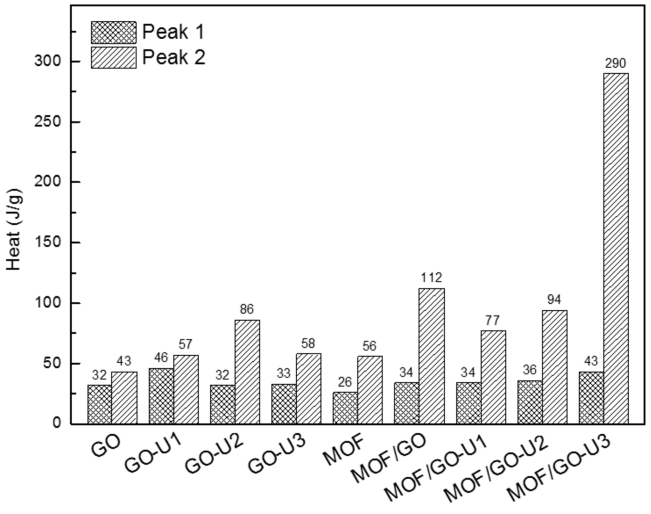

Figure 8. Comparison of calculated heat values represented by two peaks (obtained by deconvolution of the heat flow curves).

represent the cumulative heats and to get the proper perspectives on the energetic of the adsorption process, they should be analyzed considering also the measured adsorption capacities on our materials (Figure 2). In these aspects the heats measured on graphite oxide have to be considered as high and we link them to the intercalation of CO_2 between the GO layers and its interactions with polar groups. Modification with urea has a mixed effect on the heats measured on GO-U since with the introduction of amino groups some oxygen containing groups change in their chemistry and thus in the nature of polar interactions.

In the case of composites, a trend of an increase in the heats associated with the first type of adsorption centers is in agreements with an increase in the content of copper, as is shown in Figure 9. A perfect correlation is not expected since in

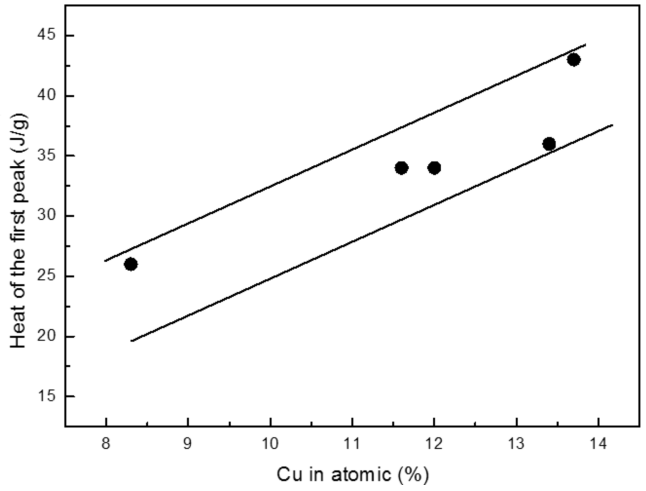

Figure 9. Dependence of the heat associated with the high energy adsorption centers on the atomic percent of copper of the surface.

this range of the surface coverage very small pores are also expected to affect the energetic of the adsorption. For the energetic effect represented by the second peak, an increase in the heats strictly follows an increase in the volume of micropores (Figure 10), which supports our proposed mechanism of adsorption on this kind of composites.

dx.doi.org/10.1021/am4006989 | ACS Appl. Mater. Interfaces 2013, 5, 4951−4959

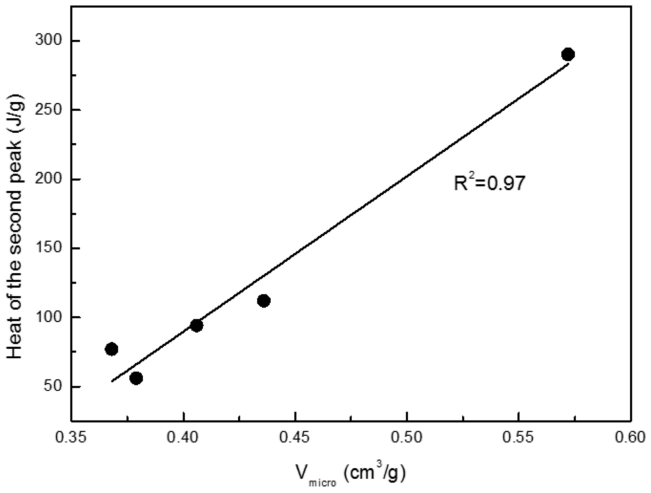

Figure 10. Dependence of the heat associated with the low energy adsorption centers on the volume of micropores.

CONCLUSIONS

New composite MOF/GO-Us were synthesized, and their CO_2 adsorption capacity at room temperature was investigated. The MOF/GO-U3 composite exhibits excellent CO_2 uptake up to 4.23 mmol/g. The synergetic effect between GO-U and Cu-BTC MOF results in the superior performance of the composites as CO_2 adsorbents. The introduction of amino group and the residual oxygen groups of GO resulted in the modified chemical environment of copper sites, led to an increase in the porosity, and caused defects in MOF crystals and thus an exposure of more unsaturated copper sites than those in the parent MOF. All of these features are beneficial for CO_2 adsorption. The results indicate that CO_2 is mainly physisorbed on the composites under dry conditions and the primary adsorption sites are the open Cu centers. Then the small micropores on the interface between MOF units and the modified graphene layers, and the cage windows, are occupied by the adsorbate molecules. The analysis of the adsorption heats suggests that the unsaturated copper sites are the stronger adsorption centers than the small micropores and the interactions between copper and CO_2 are highly specific.

ASSOCIATED CONTENT

Supporting Information

Pore size distributions and X-ray diffraction patterns for the samples studied. This material is available free of charge via the Internet at http://pubs.acs.org.

AUTHOR INFORMATION

Corresponding Author

*E-mail: tbandosz@ccny.cuny.edu. Tel.: (212) 650-6017. Fax: (212) 650-6107.

Notes

The authors declare no competing financial interest.

ACKNOWLEDGMENTS

This work was supported by ARO Grant W911NF-10-1-0039 and NSF collaborative grant CBET 1133112. The Scholarship from CSC (China Scholarship Council) for Y.Z. is highly appreciated.

REFERENCES

(1) Ghommem, M.; Hajj, M. R.; Puri, I. K. *Ecol. Model.* **2012**, *235–236*, 1–7.
(2) Hansen, J.; Johnson, D.; Lacis, A.; Lebedeff, S.; Lee, P.; Rind, D.; Russell, G. *Science* **1981**, *213*, 957–966.
(3) Choi, S.; Drese, J. H.; Jones, C. W. *ChemSusChem* **2009**, *2*, 796–854.
(4) D'Alessandro, D. M.; Smit, B.; Long, J. R. *Angew. Chem., Int. Ed.* **2010**, *49*, 6058–6082.
(5) Olajire, A. A. *Energy* **2010**, *35*, 2610–2628.
(6) Lee, Z. H.; Lee, K. T.; Bhatia, S.; Mohamed, A. R. *Renew. Sust. Energ. Rev.* **2012**, *16*, 2599–2609.
(7) Yang, H.; Xu, Z.; Fan, M.; Gupta, R.; Slimane, R. B.; Bland, A. E.; Wright, I. *J. Environ. Sci.* **2008**, *20*, 14–27.
(8) Vaidhyanathan, R.; Iremonger, S. S.; Shimizu, G. K. H.; Boyd, P. G.; Alavi, S.; Woo, T. K. *Science* **2010**, *330*, 650–653.
(9) Sharma, M.; Vyas, R.; Singh, K. *Adsorption* **2012**, 1–28.
(10) Bandosz, T. J. *Catal. Today* **2012**, *186*, 20–28.
(11) Seredych, M.; Bandosz, T. J. *J. Phys. Chem. C* **2007**, *111*, 15596–15604.
(12) Petit, C.; Levasseur, B.; Mendoza, B.; Bandosz, T. J. *Microporous Mesoporous Mater.* **2012**, *154*, 107–112.
(13) Levasseur, B.; Petit, C.; Bandosz, T. J. *ACS Appl. Mater. Interf.* **2010**, *2*, 3606–3613.
(14) Hirscher, M. *Angew. Chem., Int. Ed.* **2011**, *50*, 581–582.
(15) Furukawa, H.; Ko, N.; Go, Y. B.; Aratani, N.; Choi, S. B.; Choi, E.; Yazaydin, A. O.; Snurr, R. Q.; O'Keeffe, M.; Kim, J.; Yaghi, O. M. *Science* **2010**, *329*, 424–428.
(16) Li, J.-R.; Ma, Y.; McCarthy, M. C.; Sculley, J.; Yu, J.; Jeong, H.-K.; Balbuena, P. B.; Zhou, H.-C. *Coordin. Chem. Rev.* **2011**, *255*, 1791–1823.
(17) Millward, A. R.; Yaghi, O. M. *J. Am. Chem. Soc.* **2005**, *127*, 17998–17999.
(18) Zheng, B.; Bai, J.; Duan, J.; Wojtas, L.; Zaworotko, M. J. *J. Am. Chem. Soc.* **2010**, *133*, 748–751.
(19) Li, H.; Eddaoudi, M.; O'Keeffe, M.; Yaghi, O. M. *Nature* **1999**, *402*, 276–279.
(20) Chui, S.S.-Y.; Lo, S.M.-F.; Charmant, J.P. H.; Orpen, A. G.; Williams, I. D. *Science* **1999**, *283*, 1148–1150.
(21) Calero, S.; Martin-Calvo, A.; Hamad, S.; Garcia-Perez, E. *Chem. Commun.* **2011**, *47*, 508–510.
(22) Bao, Z.; Alnemrat, S.; Yu, L.; Vasiliev, I.; Ren, Q.; Lu, X.; Deng, S. *J. Colloid Interface Sci.* **2011**, *357*, 504–509.
(23) Yu, J.; Ma, Y.; Balbuena, P. B. *Langmuir* **2012**, *28*, 8064–8071.
(24) Liang, Z.; Marshall, M.; Chaffee, A. L. *Energy Fuels* **2009**, *23*, 2785–2789.
(25) Xie, J.; Yan, N.; Qu, Z.; Yang, S. *J. Environ. Sci.* **2012**, *24*, 640–644.
(26) Yazaydın, A. O.; Benin, A. I.; Faheem, S. A.; Jakubczak, P.; Low, J. J.; Willis, R. R.; Snurr, R. Q. *Chem. Mater.* **2009**, *21*, 1425–1430.
(27) Botas, J. A.; Calleja, G.; Sánchez-Sánchez, M.; Orcajo, M. G. *Int. J. Hydrogen Energ.* **2011**, *36*, 10834–10844.
(28) Mulfort, K. L.; Hupp, J. T. *J. Am. Chem. Soc.* **2007**, *129*, 9604–9605.
(29) Prasanth, K. P.; Rallapalli, P.; Raj, M. C.; Bajaj, H. C.; Jasra, R. V. *Int. J. Hydrogen Energ.* **2011**, *36*, 7594–7601.
(30) Gorka, J.; Fulvio, P. F.; Pikus, S.; Jaroniec, M. *Chem. Commun.* **2010**, *46*, 6798–6800.
(31) Stavitski, E.; Pidko, E. A.; Couck, S.; Remy, T.; Hensen, E. J. M.; Weckhuysen, B. M.; Denayer, J.; Gascon, J.; Kapteijn, F. *Langmuir* **2011**, *27*, 3970–3976.
(32) Xiang, Z.; Hu, Z.; Cao, D.; Yang, W.; Lu, J.; Han, B.; Wang, W. *Angew. Chem., Int. Ed.* **2011**, *50*, 491–494.
(33) Petit, C.; Huang, L.; Jagiello, J.; Kenvin, J.; Gubbins, K. E.; Bandosz, T. J. *Langmuir* **2011**, *27*, 13043–13051.
(34) Petit, C.; Mendoza, B.; Bandosz, T. J. *ChemPhysChem* **2010**, *11*, 3678–3684.
(35) Petit, C.; Mendoza, B.; Bandosz, T. J. *Langmuir* **2010**, *26*, 15302–15309.

(36) Liu, S.; Sun, L.; Xu, F.; Zhang, J.; Jiao, C.; Li, F.; Li, Z.; Wang, S.; Wang, Z.; Jiang, X.; Zhou, H.; Yang, L.; Schick, C. *Energy Environ. Sci.* **2013**, *6*, 818−823.
(37) Zhao, Y.; Seredych, M.; Zhong, Q.; Bandosz, T. J. *RSC Adv.* **2013**, DOI: 10.1039/C3RA40817E.
(38) Couck, S.; Denayer, J. F. M.; Baron, G. V.; Rémy, T.; Gascon, J.; Kapteijn, F. *J. Am. Chem. Soc.* **2009**, *131*, 6326−6327.
(39) Pinto, M. L.; Mafra, L.; Guil, J. M.; Pires, J.; Rocha, J. *Chem. Mater.* **2011**, *23*, 1387−1395.
(40) Vaidhyanathan, R.; Iremonger, S. S.; Dawson, K. W.; Shimizu, G. K. H. *Chem. Commun.* **2009**, *35*, 5230−5232.
(41) Hummers, W. S.; Offeman, R. E. *J. Am. Chem. Soc.* **1958**, *80*, 1339.
(42) Petit, C.; Burress, J.; Bandosz, T. J. *Carbon* **2011**, *49*, 563−572.
(43) Lastoskie, C. M.; Quirke, N.; Gubbins, K. E. In *Studies in Surface Science and Catalysis*; Rudziński, W., Zgrablich, G., Eds.; Elsevier: New York, 1997; Chapter 15.
(44) Wei, J.; Liao, L.; Xiao, Y.; Zhang, P.; Shi, Y. *J. Environ. Sci.* **2010**, *22*, 1558−1563.
(45) Torrisi, A.; Mellot-Draznieks, C.; Bell, R. G. *J. Chem. Phys.* **2009**, *130*, 194703−194713.
(46) Liu, Y.; Wilcox, J. *Environ. Sci. Technol.* **2012**, *47*, 95−101.
(47) Dreyer, D. R.; Park, S.; Bielawski, C. W.; Ruoff, R. S. *Chem. Soc. Rev.* **2010**, *39*, 228−240.
(48) Qian, D.; Lei, C.; Hao, G.-P.; Li, W.-C.; Lu, A.-H. *ACS Appl. Mater. Interf.* **2012**, *4*, 6125−6132.
(49) Hudson, M. R.; Queen, W. L.; Mason, J. A.; Fickel, D. W.; Lobo, R. F.; Brown, C. M. *J. Am. Chem. Soc.* **2012**, *134*, 1970−1973.
(50) Xia, Y.; Mokaya, R.; Walker, G. S.; Zhu, Y. *Adv. Energy Mater.* **2011**, *1*, 678−683.
(51) Si, X.; Jiao, C.; Li, F.; Zhang, J.; Wang, S.; Liu, S.; Li, Z.; Sun, L.; Xu, F.; Gabelica, Z.; Schick, C. *Energy Environ. Sci.* **2011**, *4*, 4522−4527.
(52) Ge, L.; Zhou, W.; Rudolph, V.; Zhu, Z. *J. Mater. Chem. A* **2013**, *1*, 6350−6358.
(53) Bae, Y.-S.; Farha, O. K.; Hupp, J. T.; Snurr, R. Q. *J. Mater. Chem.* **2009**, *19*, 2131−2134.
(54) Petit, C.; Bandosz, T. J. *Adv. Funct. Mater.* **2010**, *20*, 111−118.
(55) Zhou, C.; Cao, L.; Wei, S.; Zhang, Q.; Chen, L. *Comput. Theor. Chem.* **2011**, *976*, 153−160.
(56) Wu, H.; Simmons, J. M.; Srinivas, G.; Zhou, W.; Yildirim, T. *J. Phys. Chem. Lett.* **2010**, *1*, 1946−1951.
(57) Yang, Y.; Wang, J.; Zhang, J.; Liu, J.; Yang, X.; Zhao, H. *Langmuir* **2009**, *25*, 11808−11814.
(58) Herrera-Alonso, M.; Abdala, A. A.; McAllister, M. J.; Aksay, I. A.; Prud'homme, R. K. *Langmuir* **2007**, *23*, 10644−10649.
(59) Naumann, D. *Encyclopedia of Analytical Chemistry*; John Wiley & Sons, Ltd: New York, 2006.
(60) Smith, B. C. *Infrared spectral interpretation: a systematic approach*; CRC Press: Boca Raton, 1999.
(61) Bourlinos, A. B.; Gournis, D.; Petridis, D.; Szabó, T.; Szeri, A.; Dékány, I. *Langmuir* **2003**, *19*, 6050−6055.
(62) Chowdhury, P.; Bikkina, C.; Meister, D.; Dreisbach, F.; Gumma, S. *Microporous Mesoporous Mater.* **2009**, *117*, 406−413.
(63) Seredych, M.; Petit, C.; Tamashausky, A. V.; Bandosz, T. J. *Carbon* **2009**, *47*, 445−456.
(64) Lin, Z.; Liu, Y.; Wong, C.-P. *Langmuir* **2010**, *26*, 16110−16114.
(65) Bhatti, A. S.; Dollimore, D.; Blackmore, N. *Thermochim. Acta* **1984**, *79*, 205−216.
(66) Ding, Z.; Frost, R. L.; Kloprogge, J. T. *J. Mater. Sci. Lett.* **2002**, *21*, 981−983.
(67) Seo, Y.-K.; Hundal, G.; Jang, I. T.; Hwang, Y. K.; Jun, C.-H.; Chang, J.-S. *Microporous Mesoporous Mater.* **2009**, *119*, 331−337.